

# Amortized Inference of Multi-Modal Posteriors using Likelihood-Weighted Normalizing Flows

---

Rajneil Baruah 

*Department of Physics, SEAS, Bennett University, Greater Noida, Uttar Pradesh, India, 201310*

*Department of Physics, Bangabasi Evening College, Kolkata, West Bengal, 700011*

*E-mail: [rajneilb.physics@gmail.com](mailto:rajneilb.physics@gmail.com)*

ABSTRACT: We present a novel technique for amortized posterior estimation using Normalizing Flows trained with likelihood-weighted importance sampling. This approach allows for the efficient inference of theoretical parameters in high-dimensional inverse problems without the need for posterior training samples. We implement the method on multi-modal benchmark tasks in 2D and 3D to check for the efficacy. A critical observation of our study is the impact of the topology of the base distributions on the modelled posteriors. We find that standard unimodal base distributions fail to capture disconnected support, resulting in spurious probability *bridges* between modes. We demonstrate that initializing the flow with a Gaussian Mixture Model that matches the cardinality of the target modes significantly improves reconstruction fidelity, as measured by some distance and divergence metrics.

---

## Contents

<b>1</b>	<b>Introduction</b>	<b>1</b>
<b>2</b>	<b>Theoretical Framework: Likelihood-Weighted Normalizing Flows</b>	<b>2</b>
2.1	Normalizing Flows	2
2.2	KL Divergence, Maximum Likelihood Estimation and the Loss Function	3
2.3	Application to Posterior Estimation	3
<b>3</b>	<b>Implementation and Results</b>	<b>4</b>
3.1	Methodology	4
3.2	Implementation Details	5
3.2.1	2-Dimensional Benchmarks	5
3.2.2	3-Dimensional Benchmark	7
<b>4</b>	<b>Multi-modal Base Distributions</b>	<b>8</b>
4.1	Modality of the Base Distribution	8
4.2	Non-Gaussian Distribution	10
<b>5</b>	<b>Conclusion</b>	<b>10</b>

---

## 1 Introduction

Across diverse domains—from complex systems and finance to high-energy physics and astrophysics—scientific inquiry often relies on deriving theoretical parameters from observational data [1]. At the core of this challenge lies the *inverse problem*: inferring the posterior distribution of theoretical parameters given a set of observables [2].

Traditional approaches for posterior estimation rely on sampling algorithms such as Markov Chain Monte Carlo (MCMC) [3, 4] and Nested Sampling (NS) [5]. In astrophysics and cosmology, implementations like *emcee* [6] and *dynesty* [7] have become standard tools. While these frameworks are statistically robust, they suffer significantly from the *curse of dimensionality*. In real-world scenarios, where the parameter space is high-dimensional and the likelihood function relies on computationally expensive simulators (e.g., in particle physics phenomenology [8]), convergence can take weeks or even months.

Recent advances in machine learning have introduced *Normalizing Flows (NFs)* as a powerful alternative for probabilistic modelling [9, 10]. By learning a bijective mapping between a simple base distribution (e.g., a Gaussian) and the complex target distribution, NFs allow for exact density estimation and efficient sampling [11] from the target distribution. Modern architectures, such as RealNVP [12] and Neural Spline Flows [13], offer enough expressivity to model highly complex distributions.

However, standard training methodologies for NFs (typically Maximum Likelihood Estimation) rely on a critical assumption: that we possess a dataset of samples drawn *from the target posterior* [14]. In the context of Simulation-Based Inference (SBI) [2, 15], this often leads to approaches like Neural Posterior Estimation (NPE) [16, 17], which still require substantial simulation budgets to generate training data.

In many scientific inverse problems, this assumption does not hold. We generally possess only a generic understanding of the parameters, hence assume they belong to a uniform distribution and a “black-box” simulator that can evaluate the likelihood of a given point. If we simply train a Normalizing Flow on samples drawn from the prior, the network will trivially learn to reconstruct the prior, failing to capture the information contained in the likelihood. While Variational Inference (VI) techniques exist to approximate posteriors [18], applying them efficiently with flows to capture multi-modal structures remains an active area of research [19, 20]. Other recent efforts for estimating posterior distributions with machine learning efforts can be seen in [21, 22]

In this work, we propose a method to bridge this gap. By leveraging likelihood evaluations as *sample weights* during training—akin to Neural Importance Sampling [23]—we demonstrate that a Normalizing Flow can directly learn the transformation from a simple base density to the complex target posterior, without ever seeing a “true” posterior sample. This results in an amortized inference framework that is computationally efficient and, crucially, capable of capturing the correct topological structure (modes) of the posterior distribution.

## 2 Theoretical Framework: Likelihood-Weighted Normalizing Flows

### 2.1 Normalizing Flows

Let  $f_\phi : \mathcal{Z} \rightarrow \Theta$  be a differentiable bijection with a differentiable inverse (i.e., a diffeomorphism), parameterized by neural network weights  $\phi$ . We consider a latent space  $\mathcal{Z} \subseteq \mathbb{R}^D$  endowed with a known, tractable base density  $p_{\mathcal{Z}}(z)$  (e.g., a standard Normal distribution or a Mixture of Gaussians), and a target parameter space  $\Theta \subseteq \mathbb{R}^D$  associated with the unknown target distribution  $p(\theta)$  (or the posterior  $p(\theta|x)$ ) [9–11].

The normalizing flow  $f_\phi$  transforms the probability mass from the base distribution to the target. Crucially, because  $f_\phi$  is a diffeomorphism, it preserves the topological properties of the domain. Consequently, the support and connectivity of the modelled distribution  $q_\phi(\theta)$  are strictly constrained by the topology of the base density  $p_{\mathcal{Z}}(z)$ .

The density of the transformed variable  $\theta = f_\phi(z)$  is obtained analytically via the change of variables formula:

$$q_\phi(\theta) = p_{\mathcal{Z}}(z) \left| \det \left( \frac{\partial z}{\partial \theta} \right) \right| \quad (2.1)$$

Since  $f_\phi(z)$  is bijective, we can substitute  $z = f_\phi^{-1}(\theta)$ :

$$q_\phi(\theta) = p_{\mathcal{Z}}(z) \left| \det \left( \frac{\partial f_\phi^{-1}(\theta)}{\partial \theta} \right) \right| \quad (2.2)$$

Expressing this in logarithmic form yields:

$$\log q_\phi(\theta) = \log p_Z(z)(f_\phi^{-1}(\theta)) + \log \left| \det \left( \frac{\partial f_\phi^{-1}(\theta)}{\partial \theta} \right) \right| \quad (2.3)$$

To optimize the parameters  $\phi$ , we look to the principle of Maximum Likelihood Estimation (MLE). We seek to maximize the likelihood of the model generating the observed data, which is equivalent to minimizing the Kullback-Leibler (KL) divergence between the true distribution and the model approximation.

## 2.2 KL Divergence, Maximum Likelihood Estimation and the Loss Function

The KL divergence from a reference probability distribution  $r(\theta)$  to a model distribution  $q_\phi(\theta)$  is defined as [24]:

$$\begin{aligned} D_{\text{KL}}(r(\theta) \| q_\phi(\theta)) &= \int r(\theta) \log \frac{r(\theta)}{q_\phi(\theta)} d\theta \\ &= \int r(\theta) \log(r(\theta)) d\theta - \int r(\theta) \log(q_\phi(\theta)) d\theta \\ &= \mathbb{E}_{\theta \sim r(\theta)} [\log(r(\theta))] - \mathbb{E}_{\theta \sim r(\theta)} [\log(q_\phi(\theta))]. \end{aligned} \quad (2.4)$$

If we consider training samples  $\{\theta_i\}_{i=1}^N$  drawn i.i.d. from the distribution  $r(\theta)$ , the empirical negative log-likelihood (NLL) is given by:

$$\mathcal{L}(\phi) = -\frac{1}{N} \sum_{i=1}^N \log q_\phi(\theta_i) \xrightarrow{N \rightarrow \infty} -\mathbb{E}_{\theta \sim r(\theta)} [\log q_\phi(\theta)]. \quad (2.5)$$

Comparing eq. (2.5) and eq. (2.4), we observe that:

$$\mathcal{L}(\phi) = D_{\text{KL}}(r(\theta) \| q_\phi(\theta)) - \mathbb{E}_{\theta \sim r(\theta)} [\log(r(\theta))]. \quad (2.6)$$

Since the entropy term  $\mathbb{E}[\log(r(\theta))]$  is independent of  $\phi$ , minimizing the negative log-likelihood is mathematically equivalent to minimizing the forward KL divergence [11]:

$$\min_{\phi} (\mathcal{L}(\phi)) \iff \min_{\phi} (D_{\text{KL}}(r(\theta) \| q_\phi(\theta))). \quad (2.7)$$

## 2.3 Application to Posterior Estimation

In the context of Bayesian inference, our goal is to model the posterior distribution  $p(\theta|D)$ . According to Bayes' Theorem:

$$p(\theta | D) = \frac{p(D | \theta) p(\theta)}{p(D)}, \quad (2.8)$$

where  $p(D | \theta)$  is the likelihood,  $p(\theta)$  is the prior, and  $p(D) = Z$  is the evidence. Substituting  $r(\theta) = p(\theta|D)$  into our objective function:

$$\begin{aligned} D_{\text{KL}}(p(\theta | D) \| q_\phi(\theta)) &= \int p(\theta | D) \log \frac{p(\theta | D)}{q_\phi(\theta)} d\theta \\ &= \int \frac{1}{Z} p(\theta) p(D | \theta) \log \frac{p(\theta | D)}{q_\phi(\theta)} d\theta \\ &= \mathbb{E}_{\theta \sim p(\theta)} \left[ \frac{1}{Z} p(D | \theta) \log (p(\theta | D)) \right] \\ &\quad - \mathbb{E}_{\theta \sim p(\theta)} \left[ \frac{1}{Z} p(D | \theta) \log (q_\phi(\theta)) \right]. \end{aligned} \quad (2.9)$$

Again, retaining only the terms dependent on  $\phi$ , minimizing the divergence is equivalent to minimizing the likelihood-weighted negative log-likelihood:

$$\min_{\phi} D_{\text{KL}}(p(\theta | D) \| q_\phi(\theta)) \iff \min_{\phi} \left( -\mathbb{E}_{\theta \sim p(\theta)} \left[ \frac{p(D | \theta)}{Z} \log (q_\phi(\theta)) \right] \right). \quad (2.10)$$

In practice, we approximate this expectation using  $N$  samples drawn from the prior  $p(\theta)$ , weighted by their data-likelihood  $L(\theta_i) \equiv p(D|\theta_i)$ . The final loss function becomes:

$$\mathcal{L}(\phi) = -\frac{1}{N} \sum_{i=1}^N [L(\theta_i) \log (q_\phi(\theta_i))]. \quad (2.11)$$

### 3 Implementation and Results

To evaluate the efficacy of the proposed likelihood-weighted training, we apply the method to a set of synthetic toy problems in 2 and 3 dimensions. These problems are designed with varying degrees of topological complexity (in terms of the number of modes) to test the expressivity of the flow. To quantify the fidelity of the posterior reconstruction, we report the Kullback-Leibler ( $D_{\text{KL}}$ ) Divergence and the Average Marginal Wasserstein Distance between the true and modelled distributions.

#### 3.1 Methodology

We define a  $d$ -dimensional parameter space  $\theta \in \mathbb{R}^d$  governed by a prior  $\pi(\theta)$  (typically uniform) and a likelihood function  $L(\theta) \equiv p(D|\theta)$  given observed data  $D$ .

The training procedure is outlined in Algorithm 1. We first generate a static dataset of  $N$  samples drawn from the prior,  $\{\theta_i\}_{i=1}^N \sim \pi(\theta)$ , and evaluate their corresponding likelihoods  $w_i = L(\theta_i)$ . These likelihoods serve as importance weights. We then train a Normalizing Flow  $f_\phi : \mathcal{Z} \rightarrow \Theta$  to map a base latent distribution  $p_{\mathcal{Z}}(z)$  to the target posterior. The network is optimized by minimizing the likelihood-weighted negative log-likelihood (see eq. (2.11)). The workflow and the algorithm are shown in fig. 1.

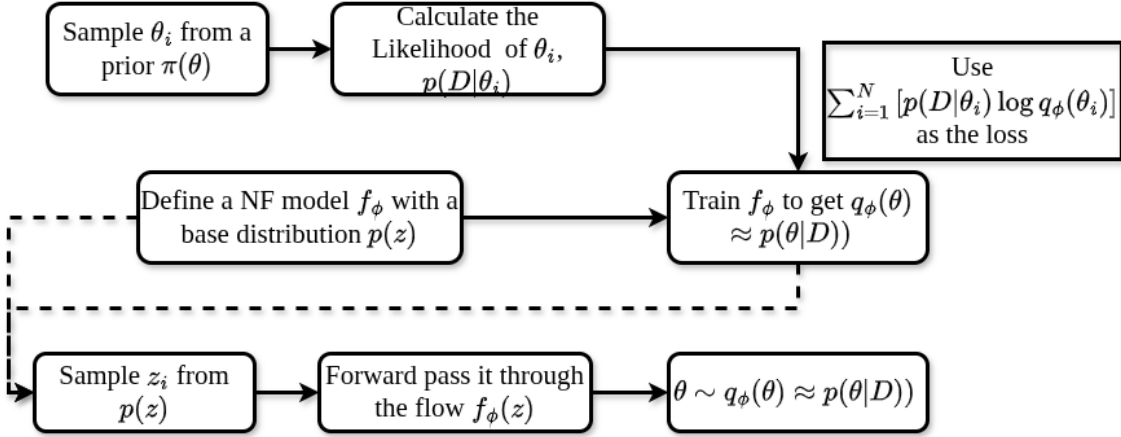


**Figure 1:** The workflow, including training the NF and then sampling from the base to pass it through the flow

---

### Algorithm 1: Likelihood-Weighted Flow Training

---

**Result:** Trained Flow parameters  $\phi^*$  approximating posterior  $p(\theta|D)$

**Inputs:** Prior  $\pi(\theta)$ , Likelihood  $L(\theta)$ , Base distribution  $p_Z(z)$ ;

**Data Generation:**

Sample  $\Theta_{\text{train}} = \{\theta_1, \dots, \theta_N\} \sim \pi(\theta)$ ;

Compute Weights  $W = \{w_1, \dots, w_N\}$  where  $w_i = L(\theta_i)$ ;

*Optional:* Pre-process  $W$  (e.g., clipping) for numerical stability;

**Training:**

**while** *not converged* **do**

Sample batch  $(\theta_b, w_b)$  from  $(\Theta_{\text{train}}, W)$ ;

Compute  $z_b = f_\phi^{-1}(\theta_b)$ ;

Compute  $\mathcal{L}(\phi) = -\frac{1}{|b|} \sum w_i \log q_\phi(\theta_i)$ ;

Update  $\phi \leftarrow \phi - \eta \nabla_\phi \mathcal{L}$ ;

**end**

---

## 3.2 Implementation Details

We utilize the `normflows` library [25] based on PyTorch. As the loss function is architecture-agnostic, we employ the Real Non-Volume Preserving (RealNVP) architecture for all experiments. Unless otherwise stated, the base distribution  $p_Z(z)$  is a standard multivariate Gaussian.

### 3.2.1 2-Dimensional Benchmarks

We define a uniform prior over the domain  $\Omega = [-12, 12]^2$ . To rigorously test mode coverage, we construct three synthetic posteriors with increasing multimodality (see fig. 2):

1. **Single-mode:** A single Gaussian centred at  $\mu_1 = [-3, 3]^\top$ .

2. **Two-mode:** An equal mixture of two Gaussians centred at  $\boldsymbol{\mu}_{2,1} = [-6, 3]^\top$  and  $\boldsymbol{\mu}_{2,2} = [6, 3]^\top$ .
3. **Three-mode:** An equal mixture of three Gaussians located at  $[-6, 6]^\top$ ,  $[6, 6]^\top$ , and  $[0, -6]^\top$ .

The covariance matrices are chosen to introduce correlation between dimensions, ensuring the task is not trivially separable.

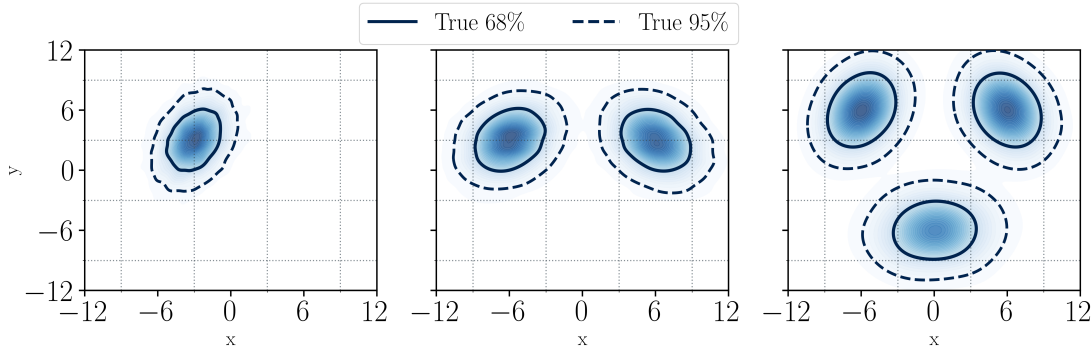


**Figure 2:** Ground truth densities for the 2D benchmark tasks. From left to right: Single-mode, Two-mode, and Three-mode posteriors constructed from Gaussian mixtures.

For each scenario, we train a RealNVP model with a standard Gaussian base distribution. Figure 3 illustrates the density of samples generated by the trained flows.

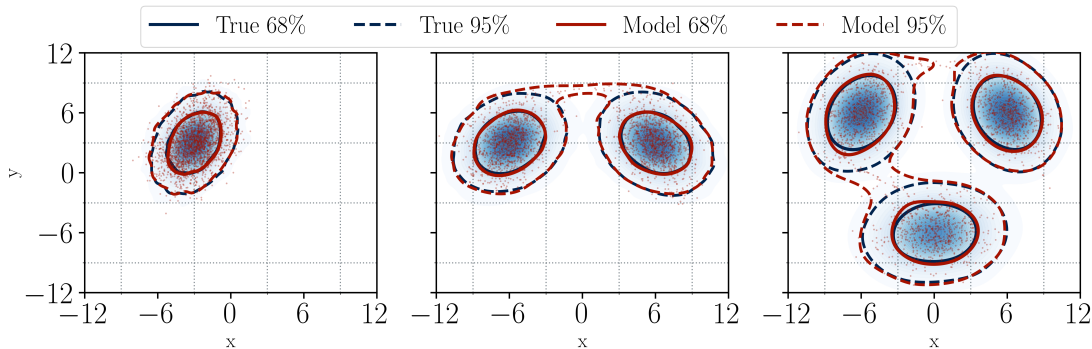


**Figure 3:** Modelled posterior distributions  $q_\phi(\theta)$  generated by the Normalizing Flow. While the single-mode posterior (Left) is captured accurately, the multi-modal cases (Center, Right) exhibit spurious “bridges” connecting the modes, a result of the topological mismatch between the unimodal base and multi-modal target.

**Quantitative Analysis** We report the KL Divergence (approximated via Monte Carlo integration) and the Average Marginal Wasserstein-1 Distance ( $W_{1,\text{avg}}$ ) in table 1.

The metrics reveal a clear trend: performance degrades as the complexity of the true posterior increases. While the KL divergence remains low ( $< 0.05$ ), indicating good global

**Table 1:** Quantitative Comparison of Posterior Reconstruction

Target Posterior	KL Divergence ( $D_{\text{KL}}$ )	Wasserstein ( $W_{1,\text{avg}}$ )
Single-Mode	0.0027	0.0904
Two-Mode	0.0171	0.1382
Three-Mode	0.0401	0.1939

overlap, the Wasserstein distance increases significantly for the multimodal cases. This degradation is a direct consequence of **topological mismatch**. The flow, being a diffeomorphism, must preserve the connectivity of the base distribution. When a unimodal base attempts to model a disconnected posterior, it is mathematically forced to draw probability mass between the modes, resulting in the "connected" artifacts observed in fig. 3.

### 3.2.2 3-Dimensional Benchmark

We extend the analysis to  $\mathbb{R}^3$  with a three-mode Gaussian mixture posterior defined as:

$$p(\boldsymbol{\theta}) = \sum_{k=1}^3 \frac{1}{3} \mathcal{N}(\boldsymbol{\theta} | \boldsymbol{\mu}_k, \boldsymbol{\Sigma}_k), \quad (3.1)$$

with means located at  $[5, 5, -5]^\top$ ,  $[5, 7, 5]^\top$ , and  $[-5, 7, 5]^\top$ , and full rank covariance matrices.

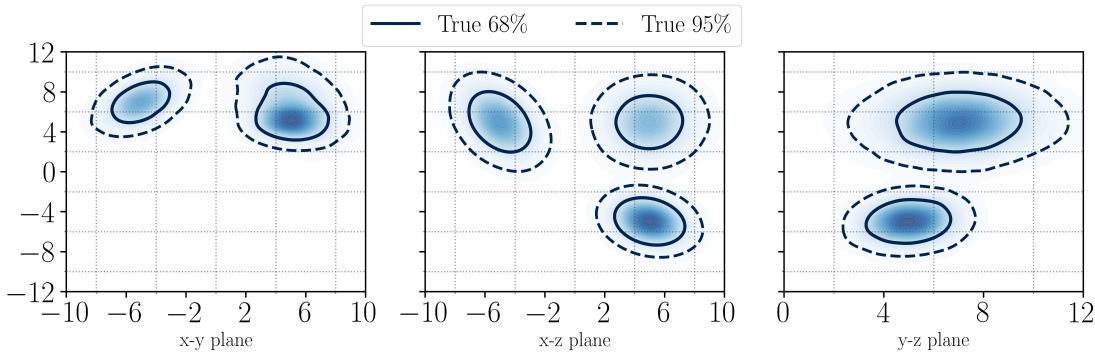


**Figure 4:** Isosurface visualization of the ground truth 3-dimensional posterior distribution, displaying three distinct modes in the parameter space. The vertical axes share identical limits and tick spacing across all panels.

We train a RealNVP with a standard multivariate normal base distribution. The results, visualized via 2D marginal projections in fig. 5, confirm the findings from the 2D case. Despite the higher dimensionality, the flow successfully locates all three modes. However, the topological constraints again force the creation of low-density bridges connecting the distinct regions of high probability.

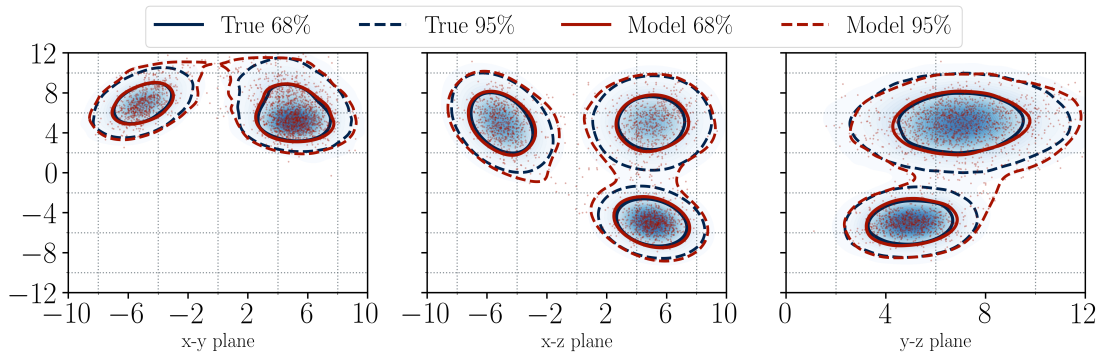


**Figure 5:** 2D Marginal projections of the modelled 3D posterior. The flow captures the location of the modes, but exhibits connectivity artifacts due to the unimodal base distribution. The vertical axes share identical limits and tick spacing across all panels

## 4 Multi-modal Base Distributions

The fundamental objective of a Normalizing Flow is to construct a parameterized diffeomorphism between a tractable base distribution and a complex target density. In section 3.2, we demonstrated that a RealNVP network trained with likelihood weights successfully approximates the posterior. However, we also observed that a unimodal base distribution can introduce topological artifacts. In this section, we systematically investigate the impact of the base distribution’s structure. Specifically, we analyse how varying the number of modes in the latent space—while maintaining a fixed network architecture—affects the fidelity of the posterior reconstruction.

### 4.1 Modality of the Base Distribution

Building on the toy problems from section 3.2, we design an experiment to test the expressivity of multi-modal base distributions. We define a set of models, denoted as  $Model - kD_i$ , where  $k$  represents the dimension of the parameter space and  $i$  indicates the number of modes in the base distribution. Specifically, for both the 2-dimensional and 3-dimensional tasks, we evaluate flows initialized with base distributions consisting of 1, 2, and 3 equally weighted Gaussian components.

The resulting modelled posteriors have been plotted in figs. 6 and 7 for the 2-D and 3-D toy problems, respectively. Comparing the plots, the modelled samples from  $Model - 2D_1$  and  $Model - 3D_1$  figs. 6 and 7 clearly show the artifact of connected modes. In contrast, samples from  $Model - 2D_2$  and  $Model - 3D_2$  figs. 6 and 7 exhibit partial separation, while  $Model - 2D_3$  and  $Model - 3D_3$  figs. 6 and 7 achieve almost complete disconnection. This shows that if the number of modes in the true posterior is higher than that of the base distribution, then there are always tails (*somewhat fat*) in the modelled posterior, maintaining the topological continuity of the base distribution. One thing to keep in mind is that, although the models are different, the target posterior distribution is the same, and hence, the for all these models, the final values of the losses remain almost identical.

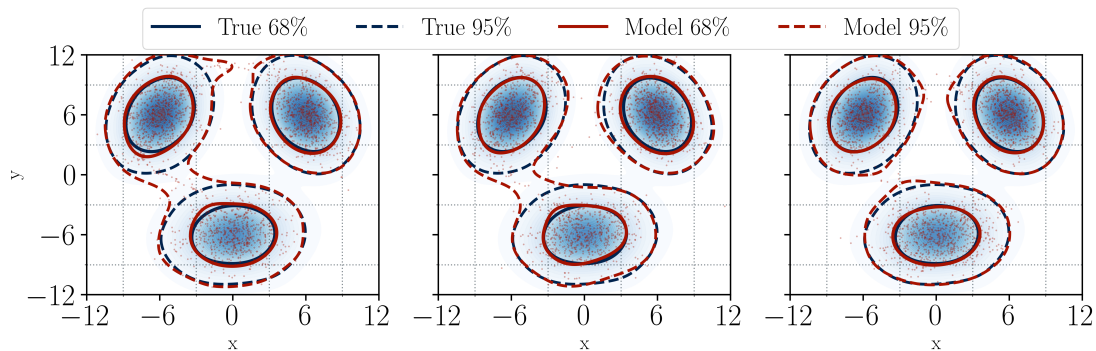


**Figure 6:** Comparison of learned posteriors from Normalizing Flows with different numbers of distinct modes in the base distribution. From Left to Right, the models have 1 base mode( $Model - 2D_1$ ), 2 base modes( $Model - 2D_2$ ) and 3 base modes( $Model - 2D_3$ ).

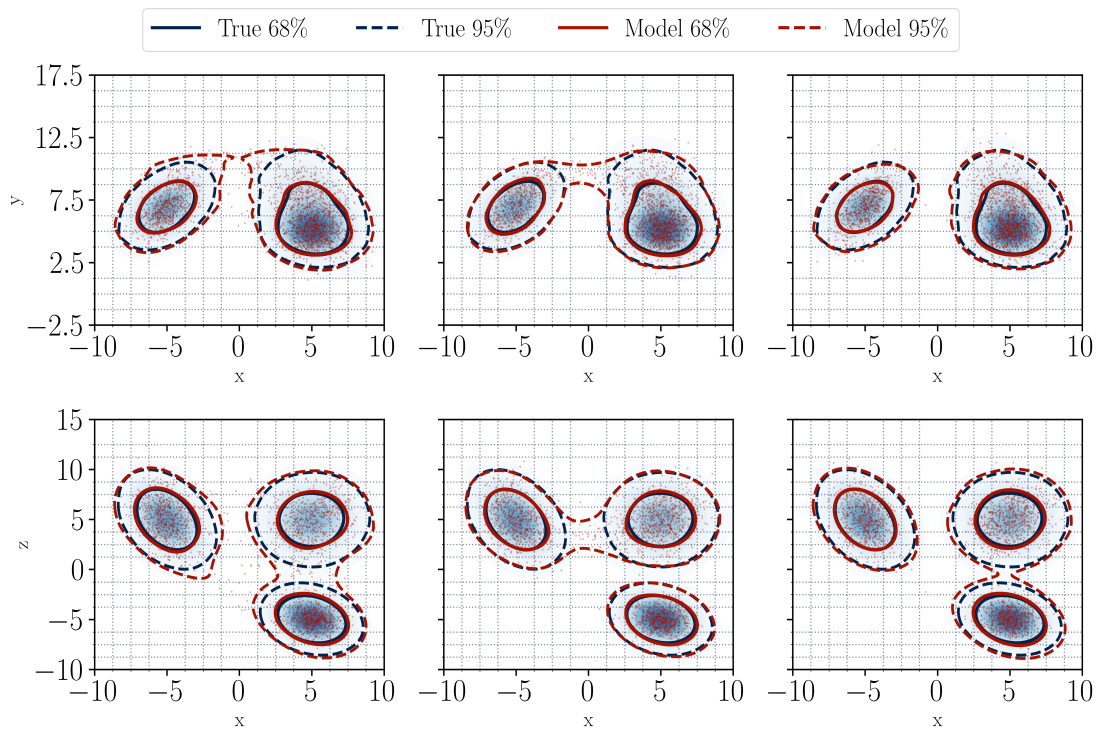


**Figure 7:** Comparison of learned posterior from Normalizing Flows with different no. of distinct modes in the base distribution. From Left to Right, the models have 1 base mode( $Model - 3D_1$ ), 2 base modes( $Model - 3D_2$ ) and 3 base modes( $Model - 3D_3$ ). The top and bottom rows are the projections on x-y plane and x-z plane, respectively.

Another critical finding is that when the number of modes in the base distribution aligns with the true posterior, the model achieves the best agreement with the truth, provided the required loss is reached for all models. This is not surprising because as

mentioned above, the modelled posteriors in such cases lose the *extra* ‘fat-tails’<sup>1</sup>. Let us look at the numbers for the toy problems above. From the table 2, it can be seen that Model – 2D<sub>3</sub> performs the best as the true number of modes in the true posterior and the base distributions are identical.

Model	Wasserstein ( $W_{1,\text{avg}}$ )	W-Sliced	KL Divergence ( $D_{\text{KL}}$ )
Model-2D <sub>1</sub>	0.1352	0.1329	0.0354
Model-2D <sub>2</sub>	0.2372	0.2767	0.0270
Model-2D <sub>3</sub>	0.0787	0.0949	0.0132

**Table 2:** Performance comparison between different 2D models.

## 4.2 Non-Gaussian Distribution

The posterior distributions considered so far are different Gaussians, either a single Gaussian or a mixture of Gaussians. In this subsection, we will look into a distribution in 3-dimensions which is a product of different non-Gaussian distributions. Given that the true posteriors are now non-Gaussian in nature and the base distributions are a mixture of Gaussians, this poses an interesting situation. We can see in fig. 8 how the modelled posterior compares with the true posterior for three different models, where, Model-nonGauss<sub>*i*</sub> corresponds to the base distribution having *i* distinct modes. The distance and divergence metrics for the three models are shown in table 3 and we can again confirm that when the modes of the base distribution and true posterior are identical, we get the best metrics.

Model	Wasserstein ( $W_{1,\text{avg}}$ )	W-Sliced	KL Divergence ( $D_{\text{KL}}$ )
Model-nonGauss <sub>1</sub>	1.6173	1.5857	0.2426
Model-nonGauss <sub>2</sub>	4.4237	4.1431	0.1116
Model-nonGauss <sub>3</sub>	0.3732	0.3880	0.0940

**Table 3:** Performance comparison of Base Models for the non-Gaussian Distribution.

## 5 Conclusion

In this work, we demonstrated that minimizing the KL-divergence from the true posterior to the modelled distribution is mathematically equivalent to maximizing the model density weighted by the data likelihood. Consequently, a Normalizing Flow trained with likelihood weights effectively approximates the posterior without requiring ground-truth samples. We validated this methodology on established 2-dimensional and 3-dimensional benchmark problems. Quantitative evaluations using both KL-divergence and Wasserstein distances confirm that the modelled distributions achieve significant overlap with the true posteriors.

<sup>1</sup>In practice, if the number of modes in the base distribution and the true posterior are high, then reaching an optimum loss while training is not very trivial in higher dimensions.

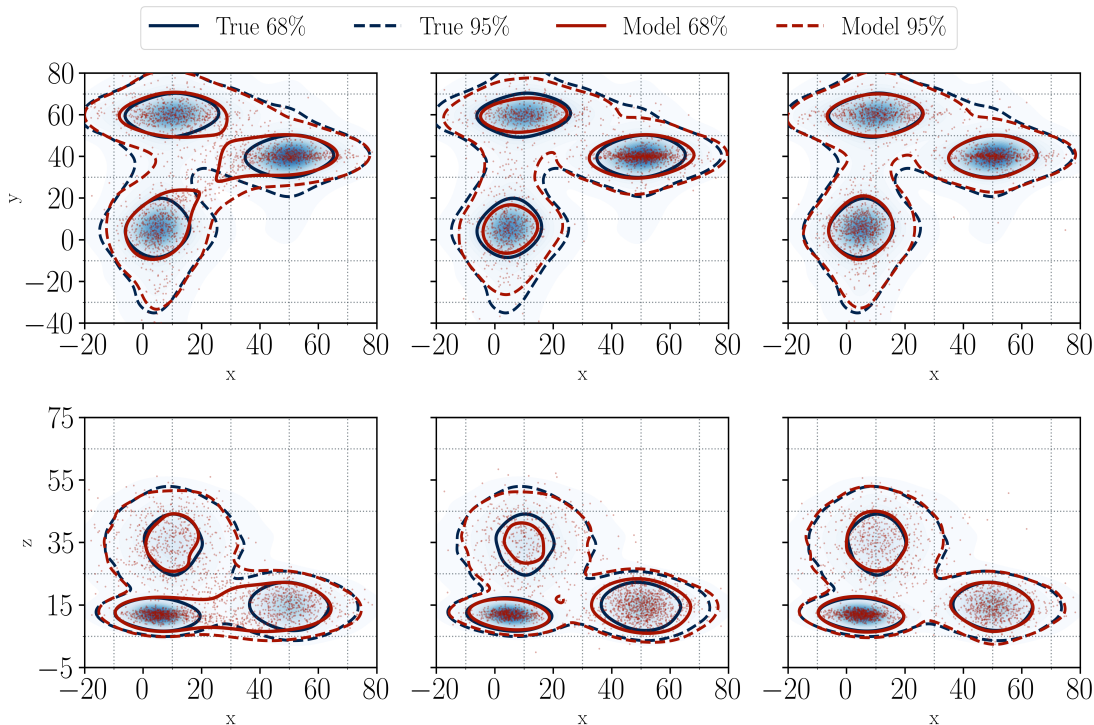


**Figure 8:** Comparison of learned posterior from Normalizing Flows with different no. of distinct modes in the base distribution, when the true posterior is a non-Gaussian distribution. From Left to Right, the models have 1 base mode(Model-nonGauss<sub>1</sub>), 2 base modes(Model-nonGauss<sub>2</sub>) and 3 base modes(Model-nonGauss<sub>3</sub>). The top and bottom rows are the projections on x-y plane and x-z plane, respectively.

Furthermore, we investigated the impact of the topology of the base distribution by replacing the standard Gaussian with a Gaussian Mixture Model (GMM). We observed that topological consistency is crucial: when the number of modes in the base distribution is lower than that of the target, the flow is forced to maintain connectivity, resulting in spurious “bridges” or tails between modes. Conversely, when the number of modes in the base and target distributions align, we achieve the lowest distance measures and the highest fidelity reconstruction. Further discussions about topology-aware generative algorithms can be found in [26, 27].

However, training flows with multi-modal base distributions presents its own challenges, particularly in higher dimensions. The network lacks explicit guidance on which base mode should map to which target mode, leading to combinatorial ambiguity and optimization instability. Thus, care must be taken to initialize or regularize these models effectively.

Ultimately, this amortized approach offers a powerful, one-shot method for posterior estimation in likelihood-accessible scenarios. Our empirical finding—that optimal performance requires topological alignment—suggests a promising avenue for future research: the development of adaptive methods to formally characterize and match the number of modes in an unknown posterior.

## Acknowledgments

The author would like to acknowledge support from ANRF (erstwhile DST-SERB), India (grant order no. CRG/2022/003208). The author thanks Sunando Kumar Patra, Bangabasi Evening College, and Subhadeep Mondal, Bennett University, for their helpful insights and guidance on the analysis of distribution topology and reconstruction fidelity, and in preparing this manuscript.

## References

- [1] A. Tarantola, *Inverse problem theory and methods for model parameter estimation*, SIAM (2005).
- [2] K. Cranmer, J. Brehmer and G. Louppe, *The frontier of simulation-based inference*, *Proceedings of the National Academy of Sciences* **117** (2020) 30055.
- [3] N. Metropolis, A.W. Rosenbluth, M.N. Rosenbluth, A.H. Teller and E. Teller, *Equation of state calculations by fast computing machines*, *The journal of chemical physics* **21** (1953) 1087.
- [4] W.K. Hastings, *Monte carlo sampling methods using markov chains and their applications*, *Biometrika* **57** (1970) 97.
- [5] J. Skilling, *Nested sampling for general bayesian computation*, *Bayesian analysis* **1** (2006) 833.
- [6] D. Foreman-Mackey, D.W. Hogg, D. Lang and J. Goodman, *emcee: the mcmc hammer*, *Publications of the Astronomical Society of the Pacific* **125** (2013) 306.
- [7] J.S. Speagle, *dynesty: a dynamic nested sampling package for estimating bayesian posteriors and evidences*, *Monthly Notices of the Royal Astronomical Society* **493** (2020) 3132.
- [8] J. Brehmer, K. Cranmer, G. Louppe and J. Pavez, *Constraining effective field theories with machine learning*, *Physical Review Letters* **121** (2018) 111801.
- [9] E.G. Tabak and E. Vanden-Eijnden, *Density estimation by dual ascent of the log-likelihood*, *Communications in Mathematical Sciences* **8** (2010) 217.
- [10] D. Rezende and S. Mohamed, *Variational inference with normalizing flows*, in *International conference on machine learning*, pp. 1530–1538, PMLR, 2015.
- [11] G. Papamakarios, E. Nalisnick, D.J. Rezende, S. Mohamed and B. Lakshminarayanan, *Normalizing flows for probabilistic modeling and inference*, *Journal of Machine Learning Research* **22** (2021) 1.
- [12] L. Dinh, J. Sohl-Dickstein and S. Bengio, *Density estimation using real nvp*, *arXiv preprint arXiv:1605.08803* (2016) .
- [13] C. Durkan, A. Bekasov, I. Murray and G. Papamakarios, *Neural spline flows*, in *Advances in Neural Information Processing Systems*, vol. 32, 2019.
- [14] G. Papamakarios, T. Pavlakou and I. Murray, *Masked autoregressive flow for density estimation*, in *Advances in Neural Information Processing Systems*, vol. 30, 2017.
- [15] J.-M. Lueckmann, J. Boelts, D. Greenberg, P. Goncalves and J. Macke, *Benchmarking simulation-based inference*, *International Conference on Artificial Intelligence and Statistics* (2021) 343.

- [16] G. Papamakarios and I. Murray, *Fast  $\epsilon$ -free inference of simulation models with bayesian conditional density estimation*, in *Advances in neural information processing systems*, vol. 29, 2016.
- [17] D. Greenberg, M. Nonnenmacher and J. Macke, *Automatic posterior transformation for likelihood-free inference*, in *International Conference on Machine Learning*, pp. 2404–2414, PMLR, 2019.
- [18] D.M. Blei, A. Kucukelbir and J.D. McAuliffe, *Variational inference: A review for statisticians*, *Journal of the American statistical Association* **112** (2017) 859.
- [19] P. Wirnsberger, A.J. Ballard, G. Papamakarios, S. Abercrombie, S. Racaniere, D.J. Rezende et al., *Targeted free energy minimization via flow-based variational inference*, in *Advances in Neural Information Processing Systems*, vol. 33, pp. 7092–7104, 2020.
- [20] L.I. Midgley, V. Stimper, G. Simidjievski, B. Schölkopf and J.M. Hernández-Lobato, *Flow annealed importance sampling bootstrap*, *arXiv preprint arXiv:2008.00392* (2020) .
- [21] R. Baruah, S. Mondal, S.K. Patra and S. Roy, *Probing intractable beyond-standard-model parameter spaces armed with machine learning*, *Eur. Phys. J. ST* **233** (2024) 2597 [2404.02698].
- [22] R. Baruah, S. Mondal, S.K. Patra and S. Roy, *Normalizing flow-assisted nested sampling on Type-II Seesaw model*, *Eur. Phys. J. C* **85** (2025) 816 [2501.16432].
- [23] T. Müller, B. McWilliams, F. Rousselle, M. Gross and J. Novák, *Neural importance sampling*, *ACM Transactions on Graphics (TOG)* **38** (2019) 1.
- [24] S. Kullback and R.A. Leibler, *On information and sufficiency*, *The Annals of Mathematical Statistics* **22** (1951) 79.
- [25] V. Stimper, D. Liu, A. Campbell, V. Berenz, L. Ryll, B. Schölkopf et al., *normflows: A pytorch package for normalizing flows*, *Journal of Open Source Software* **8** (2023) 5361.
- [26] V.S. Ngairangbam, B. Rozwoda, K. Sakurai and M. Spannowsky, *Enhancing anomaly detection with topology-aware autoencoders*, 2025.
- [27] U. Jang, S. Jha and S. Jha, *On the Need for Topology-Aware Generative Models for Manifold-Based Defenses*, *arXiv e-prints* (2019) arXiv:1909.03334 [1909.03334].